REPORT DOCUMENTATION PAGE

1a. REPORT SECURITY CLASSIFICATION UNCLASSIFIED		1b. RESTRICTIVE MARKINGS			
2a. SECURITY CLASSIFICATION AUTHORITY		3. DISTRIBUTION / AVAILABILITY OF REPORT Approved for public release, distribution unlimited.			
2b. DECLASSIFICATION / DOWNGRADING SCHEDULE					
4. PERFORMING ORGANIZATION REPORT NUMBER(S) NRL Report 9007		5. MONITORING ORGANIZATION REPORT NUMBER(S)			
6a. NAME OF PERFORMING ORGANIZATION Naval Research Laboratory	6b. OFFICE SYMBOL (If applicable) 5120	7a. NAME OF MONITORING ORGANIZATION Office of Naval Research			
6c. ADDRESS (City, State, and ZIP Code) Washington, DC 20375-5000		7b. ADDRESS (City, State, and ZIP Code) Arlington, VA 22217-5000			
8a. NAME OF FUNDING / SPONSORING ORGANIZATION Office of Naval Research	8b. OFFICE SYMBOL (If applicable)	9. PROCUREMENT INSTRUMENT IDENTIFICATION NUMBER			

8c. ADDRESS (City, State, and ZIP Code) Arlington, VA 22217-5000	10. SOURCE OF FUNDING NUMBERS			
	PROGRAM ELEMENT NO. 61153N	PROJECT NO. RR015-09-41 RR032-04-01	TASK NO.	WORK UNIT ACCESSION NO. DN080-101 DN091-274

11. TITLE (Include Security Classification)

The Canted Spectral Transform and Its Properties

12 PERSONAL AUTHOR(S)
Gerlach, A. A., Flowers, K. D., Anderson, W. L., and Kunz, E. L.

13a. TYPE OF REPORT Interim	13b. TIME COVERED FROM _____ TO _____	14. DATE OF REPORT (Year, Month, Day) 1986 November 14	15. PAGE COUNT 24

16. SUPPLEMENTARY NOTATION

17. COSATI CODES			18. SUBJECT TERMS (Continue on reverse if necessary and identify by block number)
FIELD	GROUP	SUB-GROUP	Spectral transforms Acoustic signal processing Detection and estimation Statistical analysis

19 ABSTRACT (Continue on reverse if necessary and identify by block number)

A generalized spectral transform is defined by extending the kernel of the conventional sectionalized Fourier transform (SFT). The generalized transform accumulates signal energy along narrow dynamic spectral channels, which may be made to conform to the instantaneous-frequency dynamics of a given signal. This property may be used to achieve optimum detection of a deterministically known signal or to estimate the spectral dynamics of an unknown signal over the temporal limits of the transform.

As an initial step toward achieving the general spectral transform, the canted spectral transform (CST) is defined by using a quadratic phase kernel. The statistical properties of the CST are derived and compared with those of the conventional SFT. In general, the use of shaded windows in the CST does not appear to be advantageous and can degrade the selectivity of the transform in estimating the signal-frequency dynamics. Statistical distributions of the peak cant variable for an idealized signal in Gaussian noise provide a basis for determining the performance of the CST in practical applications.

20. DISTRIBUTION / AVAILABILITY OF ABSTRACT ☐ UNCLASSIFIED/UNLIMITED ☒ SAME AS RPT. ☐ DTIC USERS	21. ABSTRACT SECURITY CLASSIFICATION UNCLASSIFIED	
22a. NAME OF RESPONSIBLE INDIVIDUAL Dr. Albert A. Gerlach	22b. TELEPHONE (Include Area Code) (202) 767-2109	22c. OFFICE SYMBOL 5120

DD FORM 1473, 84 MAR   83 APR edition may be used until exhausted.   SECURITY CLASSIFICATION OF THIS PAGE
All other editions are obsolete.

Naval Research Laboratory

Washington, DC 20375-5000 . **NRL Report 9007** . November 1986

The Canted Spectral Transform and Its Properties

A. A. GERLACH, K. D. FLOWERS,
W. L. ANDERSON, AND E. L. KUNZ

Acoustics Division

CONTENTS

THE CANTED SPECTRAL TRANSFORM
AND ITS PROPERTIES

INTRODUCTION

Spectral transforms play a major role in modern signal processing and analysis. This role will undoubtedly be expanded in the future as a consequence of advances in microelectronics and computer technologies. The most common spectral transform used in practice is the discrete sectionalized Fourier transform (SFT) which evolved with the advent of the fast Fourier transform (FFT) algorithm of Cooley and Tukey [1,2]. The FFT algorithm opened the door to high-speed coherence estimation in low-frequency (acoustic) applications through its use as an SFT [3-6]. In application, the SFT accumulates a signal energy along narrow spectrally invariant channels (or frequency bins) over the temporal limits of the transform integration interval. This restriction on signal-spectral dynamics is imposed by the Fourier kernel, $\exp\{-i2\pi ft\}$. One may therefore surmise that this restriction is rather arbitrary, and that one may accumulate signal energy along any dynamic spectral path by choosing a suitable kernel function to use in the transform. Suppose, for example, that one chooses a kernel, $\exp\{-i\Psi(t)\}$, where

$$\Psi(t) = 2\pi \sum_{n=0}^{N-1} \eta_n t^{n+1} = 2\pi \left[\eta_0 t + \eta_1 t^2 + \ldots + \eta_{N-1} t^N \right]. \tag{1a}$$

The transform of a signal using $\Psi(t)$ as a kernel will accumulate energy over dynamic spectral paths

$$f(t) = \frac{1}{2\pi} \dot{\Psi}(t) = \sum_{n=0}^{N-1} (n+1)\eta_n t^n. \tag{1b}$$

Here $\dot{\Psi}(t)$ is the time derivative of the generalized phase function $\Psi(t)$. It should be evident, therefore, that for a narrowband signal $s(t) = A \sin\theta(t)$ whose instantaneous frequency satisfies

$$\frac{1}{2\pi} \dot{\theta}(t) = \sum_{n=0}^{N-1} \frac{f^{(n)}(0)}{n!} t^n, \tag{2a}$$

over $0 \leqslant t \leqslant T$, the magnitude square of its spectral transform reduces to

$$\frac{1}{T} \left| \int_0^T s(t) e^{-i\Psi(t)} dt \right|^2 = \frac{1}{T} \int_0^T s^2(t) dt, \tag{2b}$$

for

$$\eta_n = f^{(n)}(0) / (n+1)! \tag{2c}$$

With foreknowledge of the spectral dynamics of a given signal, the kernel parameters η_n of the generalized transform may be chosen to provide an effective matched filter for the signal. Without this foreknowledge, the kernel parameters may be varied to search for the set that maximizes the transform output; thus providing an estimate of the detected signal spectral dynamics.

1

Although sound in principle, the generalized spectral transform becomes increasingly computationally intensive as the order of the phase polynomial becomes large. However, extending the phase kernel from linear to quadratic is a reasonable step to further the cause of the generalized concept in spectral transforms.

The utility of the quadratic phase kernel has recently received some degree of recognition. Wolcin [7] has demonstrated that when the spectral trajectory of a signal can be adequately modeled by a continuous, piecewise linear function of time, the maximum a posteriori estimate of the narrowband signal (not surprisingly) results in exponential quadratic phase functions. George Rogers, at TRW, Inc., subsequently determined that the use of the quadratic phase kernel in place of the conventional linear Fourier kernel could significantly improve the detection of particular classes of spectral dynamic signals propagating in the ocean medium [8]. The objective of this report is to study the properties of the spectral transform that employs the quadratic phase kernel, in a preliminary effort to determine its utility in practical applications. This form of the spectral transform will be called the canted spectral transform (CST); in that it accumulates signal energy along spectral paths that may be canted (or linearly sloping) with respect to time. The discrete form of the transform using the combined Fourier-Fresnel kernel is also referred to (by Rogers) as the slide-fast Fourier transform or S-FFT.

FORMULATION OF THE CST

The discrete form of the CST to be studied in this report is*

$$F(k,\nu) = \frac{1}{W} \left| \sum_{n=0}^{N-1} w_n s_{n_0+n} \, e^{-i2\pi \left[k\frac{n}{N} + \frac{\nu}{2}\left(\frac{n}{N}\right)^2 \right]} \right|, \tag{3}$$

where

s_j are the signal samples over the interval $n_0 \leqslant j < n_0 + N - 1$,
$k = 0,1,2,3,\ldots,N-1$ is the frequency index,
$\nu = 0,\pm 1, \pm 2, \pm 3, \ldots,\pm\nu_{max}$ is the cant (or frequency-slide) index,
n is the time index (or sample number) relative to n_0,
n_0 is the initial time index,
$w_n = w_{N-n}$ is the window function over $0 \leqslant n \leqslant N-1$,

and

$$W = \sum_{n=0}^{N-1} w_n \text{ is the windowed signal-averaging factor.}$$

The signal $s(t)$ is assumed to be uniformly sampled over time increments Δt. The transform-integration time T is therefore $N\Delta t$. The bin width of the spectral channels is $1/T$, centered at $f = k/T$. The frequency slide, $\dot{f} = \Delta f/T = \Delta k/T^2$, of the spectral channels is ν/T^2. The cant ν is the integer number Δk of frequency bins shifted over the transform-integration time T. The factor W is equal to N for the conventional rectangular window and equals $N/2$ for the Hanning window. The spectral channel width $1/T$ is generally chosen to encompass the short-term bandwidth of the narrowband signal components of interest. And the range of the cant variable is chosen to encompass the anticipated frequency shift of the signal components over the transform-integration time. As a consequence, the class of narrowband signals most suitable for analysis by the CST is that whose member's instantaneous frequency deviates from linear over time T no greater than approximately $1/T$.

---

*Although the discrete CST would be complex and not include the absolute value signs, it is convenient to consider only the magnitude of the transform in this early study of its general properties.

THE CHARACTERISTIC FUNCTION Z(x,y)

Since the CST is structured to accumulate signal energy along canted or sloping channels in the frequency-time plane, let $s(t)$ be a signal whose instantaneous frequency varies linearly with time. That is, let

$$s_{n_0+n} = e^{i\left[2\pi k_0 \frac{n}{N} + \pi \nu_0 \left(\frac{n}{N}\right)^2 + \theta_0\right]},$$ (4)

where

$k_0 = f_0 T$

f_0 is the instantaneous frequency of $s(t)$ at $t_0 = n_0 \Delta t$

$\nu_0 = \dot{f}_0 T^2$

$\dot{f}_0$ is the time derivative of the instantaneous frequency at t_0

and

θ_0 is a constant phase term.

In this event, from Eqs. (3) and (4), the CST becomes

$$F(k,\nu) = \frac{1}{W} \left| \sum_{n=0}^{N-1} w_n e^{-i\pi\left[2\left(k-k_0\right)\frac{n}{N} + \left(\nu-\nu_0\right)\left(\frac{n}{N}\right)^2\right]} \right|.$$ (5)

Letting $x = k - k_0$ and $y = \nu - \nu_0$ defines the characteristic function of the CST as

$$Z(x,y) = \frac{1}{W} \left| \sum_{n=0}^{N-1} w_n e^{-i\pi\left[2x\frac{n}{N} + y\left(\frac{n}{N}\right)^2\right]} \right|.$$ (6)

The CST characteristic function $Z(x,y)$ is a quasi-continuous function of the variables x and y (since k_0 and ν_0 need not be integers), and it serves to demonstrate some of the properties of the CST.

Symmetry Relations

Replacing x by $-x$ and y by $-y$ in Eq. (6) gives the symmetrical relationship

$$Z(-x,-y) = Z(x,y).$$ (7a)

The above symmetry implies that paired values k, k' and ν, ν' (corresponding to pairs $x, -x$ and $y, -y$ respectively) must satisfy the relations

$$\bar{k} = (k + k')/2 = k_0,$$ (7b)

and

$$\bar{\nu} = (\nu + \nu')/2 = \nu_0.$$ (7c)

Consequently, k_0 and ν_0 must be integer multiples of 1/2 since k, k', ν, and ν' are integers. The geometric interpretation is that k and k' are spectral bins symmetrically located about k_0 with cants ν

and ν' such that the resulting spectral trajectories intersect the spectral trajectory of the signal k_0, ν_0 at a common point.

Note from Eq. (5) that the CST is dependent on only the differences $k - k_0$ and $\nu - \nu_0$. Thus one can determine the canted transform of any linear frequency-slide signal (including the cw signal) by computing the conventional Fourier transform of a canted signal whose parameters are k_0 and $\nu_o - \nu$. This is apparent from the form of the CST in Eq. (3), which can be interpreted as the conventional Fourier transform of a signal modified by the phase kernel, $\exp\{-i\pi\nu n^2/N^2\}$.

Letting n go to $N - n$ in Eq. (6), and using the identity $w_{N-n} = w_n$, the CST characteristic function becomes

$$Z(x,y) = \frac{1}{W}\left| \sum_{n=0}^{N-1} w_n\, e^{i\pi\left[2(x+y)\frac{n}{N} - y\left(\frac{n}{N}\right)^2\right]} - w_0\left[1 - e^{i\pi(2x+y)}\right] \right|. \tag{8a}$$

For typically large values of N, the second term is insignificant in comparison to the summed term and can be ignored. Therefore,

$$Z(-x-y,y) = Z(x,y) = Z(x+y,-y) = Z(-x,-y). \tag{8b}$$

Thus, the two values k and $k' = 2k_0 + \nu_0 - \nu - k$ (corresponding to x and $-x-y$) will give the same value for the characteristic function. In geometric terms, given the values k_0, ν_o, and ν, any two values of k whose arithmetic mean is

$$\bar{k} = (k + k')/2 = k_0 + (\nu_0 - \nu)/2 \tag{8c}$$

will give the same value for the characteristic function. Writing the above equation as

$$\bar{k} + \nu/2 = k_0 + \nu_0/2 \tag{8d}$$

reveals that the spectral trajectory originating at $\bar{k}$ with cant ν intersects the trajectory originating at k_0 with cant ν_0 at its midpoint. Consequently, the trajectories originating at k and k' will intersect the trajectory of the relevant signal $s(t)$ at points symmetrically distributed about its midpoint. Since k and ν are integers, it is necessary that $2k_0 + \nu_0$ be an integer.

Translation of the Temporal Index

Translating the temporal index of the CST characteristic function by α gives the interesting result that

$$Z'(x,y;\alpha) = \frac{1}{W}\left| \sum_{n=0}^{N-1} w_n\, e^{-i\pi\left[2x\left(\frac{n}{N}-\alpha\right) + y\left(\frac{n}{N}-\alpha\right)^2\right]} \right|,$$

$$= \frac{1}{W}\left| \sum_{n=0}^{N-1} w_n\, e^{-i\pi\left[2(x-\alpha y)\frac{n}{N} + y\left(\frac{n}{N}\right)^2\right]} \right|, \tag{9a}$$

$$= Z(x-\alpha y,y).$$

Thus, translating the time index n by αN is equivalent to translating the x variable by αy. In particular,

$$Z'(0,y;-x/y) = Z(x,y)$$

$$= \frac{1}{W} \left| \sum_{n=0}^{N-1} w_n \; e^{-i\pi y \left(\frac{n}{N} + \frac{x}{y} \right)^2} \right|. \tag{9b}$$

Thus, one can compute the characteristic function using only the quadratic phase term by appropriate translation of the time index.

A study of Eq. (9b) reveals that the range of phase excursion over n is minimized when $x = -y/2$. The characteristic function for minimum phase excursion may be written as

$$Z(-y/2,y) = \frac{1}{W} \left| 2 \sum_{n=0}^{N/2} w_{N/2+n} \; e^{-i\pi y \left(\frac{n}{N} \right)^2} - \left(1 + w_0 e^{-i\pi y/4} \right) \right|,$$

$$\approx \frac{2}{W} \left| \sum_{n=0}^{N/2} w_{N/2+n} \; e^{-i\pi y \left(\frac{n}{N} \right)^2} \right|. \tag{9c}$$

Topology of Z(x,y)

To map the topology of the CST characteristic function over the x, y plane, the functional form given in Eq. (9b) may be used to give

$$Z(x,y) = \left[\left| Z_R(x,y) \right|^2 + \left| Z_I(x,y) \right|^2 \right]^{1/2}, \tag{10a}$$

where

$$Z_R(x,y) = \frac{1}{W} \sum_{n=0}^{N-1} w_n \; \cos \left[\pi y \left(\frac{n}{N} + \frac{x}{y} \right)^2 \right],$$

$$\approx \frac{N}{W} \int_0^1 w(\xi) \; \cos \left[\pi y \left(\xi + \frac{x}{y} \right)^2 \right] d\xi, \tag{10b}$$

and

$$Z_I(x,y) = \frac{1}{W} \sum_{n=0}^{N-1} w_n \; \sin \left[\pi y \left(\frac{n}{N} + \frac{x}{y} \right)^2 \right],$$

$$\approx \frac{N}{W} \int_0^1 w(\xi) \; \sin \left[\pi y \left(\xi + \frac{x}{y} \right)^2 \right] d\xi. \tag{10c}$$

Although the above functions are undefined for $y=0$, the singularity is removable, resulting in the form of the conventional Fourier transform of the window function.

Rectangular Window

For a rectangular window function, a closed form of the solution is obtained involving the Fresnel sine and cosine integrals $S(\cdots)$ and $C(\cdots)$ as follows:

$$Z_R(x,y) = \frac{C(\beta_2 + \beta_1) - C(\beta_1)}{\beta_2}, \tag{11a}$$

$$Z_l(x,y) = \frac{S(\beta_2+\beta_1) - S(\beta_1)}{\beta_2} , \tag{11b}$$

where

$$\beta_1 = \pm \sqrt{\frac{2}{|y|}} \ |x| \ \text{ and } \ \beta_2 = \sqrt{2|y|}, \tag{11c}$$

and where the sign of β_1 is positive when x and y have the same sign and negative when their signs differ. This result for a linear slide frequency was demonstrated in Ref. 6 and has also been derived and demonstrated by Rogers [8] in his unpublished work on the slide-FFT. For $x=0$ or $x=-y$, the characteristic function reduces to

$$Z(0,y) = Z(-y,y) = \frac{\sqrt{S^2(\beta_2) + C^2(\beta_2)}}{\beta_2} , \tag{12a}$$

and for $x=-y/2$,

$$Z(-y/2,y) = \frac{\sqrt{S^2(\beta_2/2) + C^2(\beta_2/2)}}{\beta_2/2} . \tag{12b}$$

Figure 1 shows graphical plots of the CST characteristic function for the rectangular window. To achieve the realism of the CST, the topology is mapped over integer increments of x and y about initial offsets of either 0 or 1/2. As a visual aid, the discrete values along the x axis are connected by straight lines. The offsets of 1/2 in either or both the x and y axis are intended to depict the effect of noninteger values for the signal parameters k_0 and ν_0 on the resulting topology. In the upper left-hand diagram, the parameters k_0 and ν_0 are both integers. Consequently, a peak value of 1 is achieved for $x=y=0$. In the upper right-hand diagram, the parameter k_0 is depicted to be an odd multiple of 1/2. That is, the initial frequency is depicted to start at the edge of a CST bin, while the cant ν_0 remains an integer. In the lower left-hand diagram, the parameter k_0 is an integer while the cant parameter ν_0 is depicted to be an odd multiple of 1/2. In this situation, the cant can never be fully compensated by the integer variable ν. The lower right-hand diagram depicts the situation where both k_0 and ν_0 are odd multiples of 1/2. In reality, the two scale offsets can fall anywhere between $\pm$ 1/2. In Fig. 1 only the extreme offsets are depicted. The illustrations demonstrate the functional symmetry derived in the earlier analysis.

Hanning Window

To study the effect of a shading window function on the CST, the popular Hanning window is used. In this case the window function w_n is $\sin^2(\pi n/N)$ and $N/W = 2$. Unfortunately, a closed-form solution is not available; however, by using Eq. (10), graphical plots of the characteristic function were computed and are displayed in Fig. 2. The rationale for the four diagrams is identical to that described for the case of the rectangular window function.

Cant Selectivity

A study of the characteristic function topology for the two window functions (Figs. 1 and 2) reveals marked differences in the cant selectivity. In the case of the rectangular window (commonly called the no window case since $w_n = 1$ over the integration interval), the peak of the contour is more sharply defined. The variation of the contour over the x,y plane is, however, more erratic. At the larger values of y, the spread of the peak along the x axis is relatively broad. On the other hand, the topology of the characteristic function for the Hanning window is relatively smooth, and it displays a
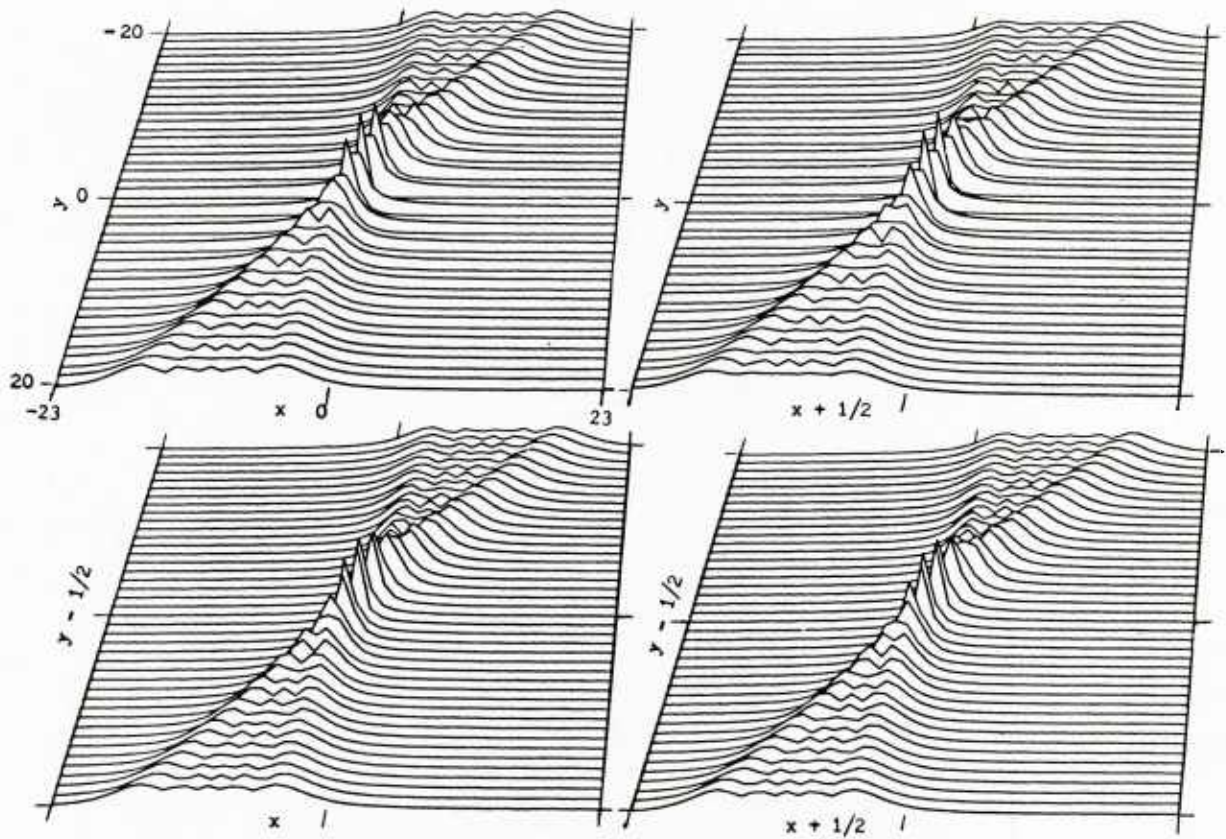
Fig. 1 — Topology of the CST characteristic function $Z(x,y)$ for a rectangular window. The upper left-hand diagram illustrates the case when k_0 and ν_0 are integers. In the upper right-hand diagram, ν_0 is an integer but k_0 is an odd multiple of 1/2; that is, k_0 occurs at a bin edge. The two peaks occur for $y = \nu - \nu_0 = \pm 1$. In the lower left-hand diagram, k_0 is an integer but ν_0 is an odd multiple of 1/2; that is, ν_0 is midway between two cant values of ν. The two central peaks are equal and occur for $y = \nu - \nu_0 = \pm 1/2$. In the lower right-hand diagram, both k_0 and ν_0 are odd multiples of 1/2.
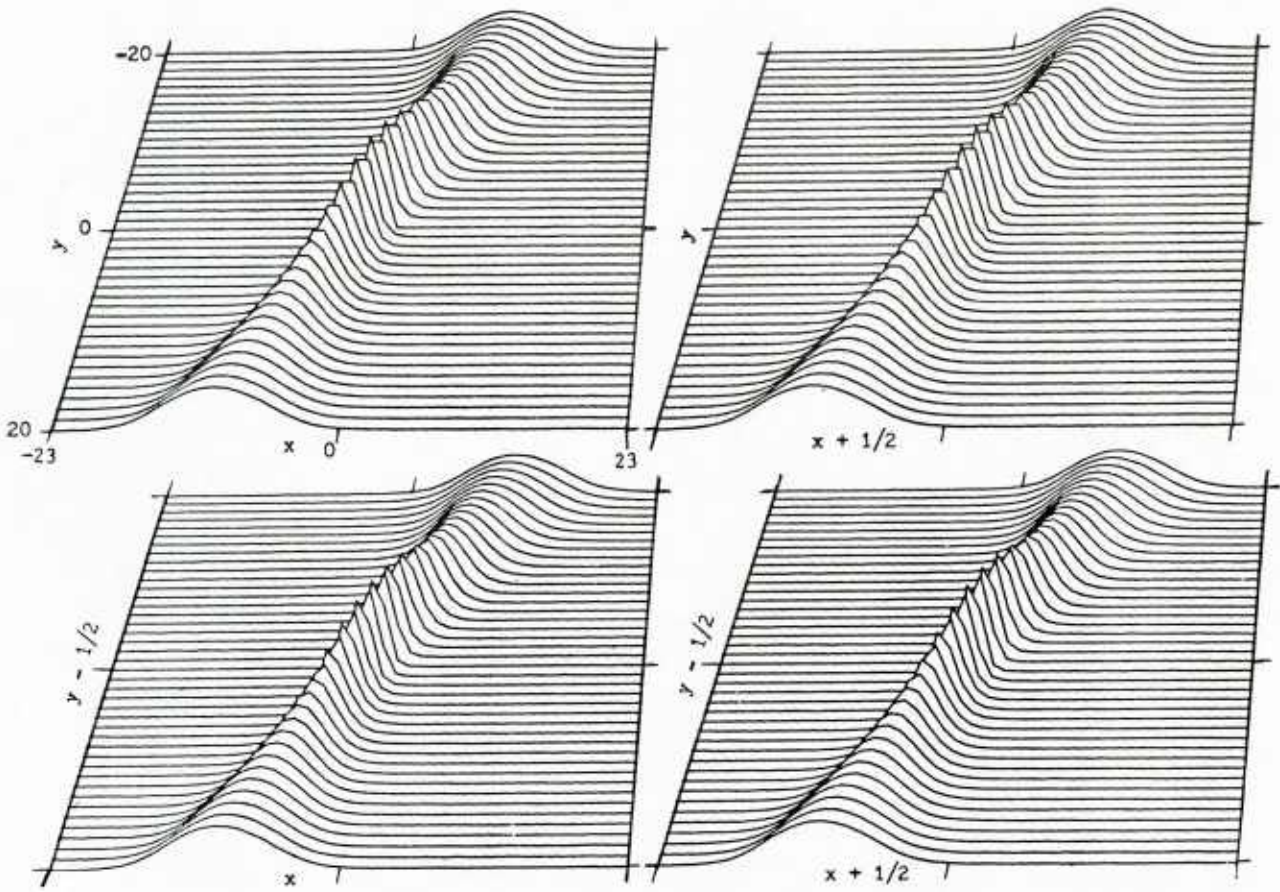
Fig. 2 — Topology of the CST characteristic function $Z(x,y)$ for a Hanning window. The rationale and peak characteristics of the four diagrams are the same as described in Fig. 1. The topology for the shaded window is, however, more smooth. And, the peak of the topology decays less rapidly (along the line of minimum phase excursion $x=-y/2$) as the absolute value of y increases.

more gradual falloff along the line $y = -2x$. For the purpose of estimating the cant of a linear frequency-slide signal, the rectangular window would prove superior; particularly, in a noisy environment.

To obtain a quantitative measure of the cant selectivity, the peak value of the characteristic function over x was computed as a function of y for the two window functions. These values involve offsets within $\pm 1/2$ about integer values of x and y. The results are plotted in Fig. 3 as a function of integer values of the cant variable. The diagrams display the expected value (small circle) and the range of variation of $Z(x,y)$ due to the random offsets. The value of $Z(x,y)$ at each y in Fig. 3 are uniquely dependent on the specific offsets. Thus, the indicated variations along the abscissa are not independent but are highly correlated. The results demonstrate the superiority of the rectangular window in resolving the cant of a narrowband signal in a noisy background environment.
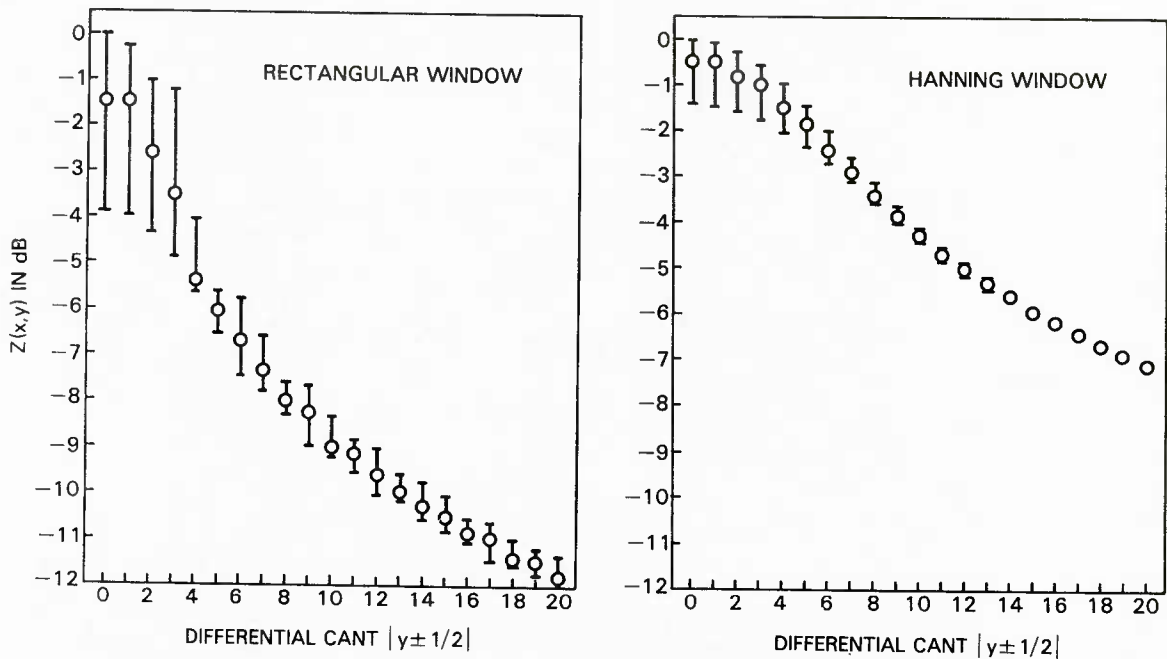

Fig. 3 — Cant selectivity of the CST characteristic function $Z(x,y)$ for the rectangular and Hanning windows. The vertical lines depict the range of variation in CST output for k_0 and ν_0 uniformly distributed over $\pm 1/2$ about given integers. The specific values at points along the abscissa are not independent but perfectly correlated. That is, given the values for k_0 and ν_0, the CST outputs are uniquely determined at the points along the abscissa and will fall within the range indicated in the figure.

CST STATISTICS FOR A RANDOM NOISE SIGNAL

Let $F_i(k,\nu)$ be the CST, given in Eq. (3), of a sample signal randomly selected from an ensemble of zero-mean Gaussian functions with standard deviation σ. Define $\tilde{\nu}$ as the specific value of ν whereby $F_i(k,\nu) \leqslant F_i(k,\tilde{\nu})$ for a given value of k. Therefore, $F_i(k,\nu)$ and $F_i(k,\tilde{\nu})$ are samples of a random function whose statistics are studied in the following paragraphs. For purposes of the study, the CST size is assumed to be very large, much larger than the range over which the cant ν is varied.

Distribution of $F_i(k,\nu)$

For a Gaussian signal, it is known that $F_i(k,o)$ is a Rayleigh-distributed random variable with mean proportional to $\sqrt{\pi/2}\,\sigma$ and variance equal to $4/\pi - 1$ times the square of the mean. Computer runs over a large set of Gaussian inputs have verified that $F_i(k,\nu)$ is Rayleigh distributed and identical for each k and ν (as expected).

Distribution of $F_i(k, \tilde{\nu})$

To study the distribution of the peak CST for a Gaussian noise input let

$$\chi_j = F_i(k, \nu_j), \tag{13a}$$

where ν_j is selected from the set $\{\nu\}$. Consider the set $\chi_1, \chi_2, \ldots, \chi_n$ and denote $\tilde{\chi} = F_i(k, \tilde{\nu})$ as a member of the set; such that, $\chi_j \leqslant \tilde{\chi}$ for $j = 1, 2, \ldots, n$. Now, it has been shown that when the distribution functions for the set of χ_j are identical and independent, the distribution function for $\tilde{\chi}$ is simply [9]

$$F_{\tilde{\chi}}(z) = [F_\chi(z)]^n,$$

where $F_{\tilde{\chi}}(z)$ is the probability that $\tilde{\chi}$ is less than z and $F_\chi(z)$ is the probability that χ_j is less than z for a given ν_j. Since χ is Rayleigh distributed,

$$F_{\tilde{\chi}}(z) = (1-p)^n,$$
$$= \sum_{j=0}^{n} (-1)^j \, _nC_j p^j, \tag{14a}$$

where $_nC_j$ is the binomial coefficient and p is the complement Rayleigh distribution, $\exp\{-z^2/2\sigma^2\}$, or the probability that $z \leqslant \chi$. The complement distribution function for $\tilde{\chi}$ as a function of p is therefore

$$P_{\tilde{\chi}}(p) = \sum_{j=1}^{n} (-1)^{j-1} \, _nC_j p^j,$$
$$= np\left[1 - \frac{n-1}{2!} p + \frac{(n-1)(n-2)}{3!} p^2 - \ldots \right]. \tag{14b}$$

Thus when p is less than $0.2/(n-1)$, the complement distribution function for $\tilde{\chi}$ approximates np.

Curves of the idealized complement distribution function are shown in Fig. 4 for several values of n. Since these curves are based on independent distribution functions for the set χ_j, computer runs were made to determine the difference between the actual and idealized complement distribution function for the same values of n. This proved to be a rather formidable task due to the large sample size required to achieve accurate measures of the function. However, sufficient data were achieved to show that the difference is quite small. In every case, the actual probability proved to be slightly less than the data given in Fig. 4; particularly in the range of p between 10^{-1} and 10^{-4}. The results for $n=41$ (where the accuracy is higher than for the lower values of n) are shown in Fig. 5. The results for lower values of n are comparable to those shown in the figure for values of p less than about 10^{-2}. The difference is that as n becomes smaller, the curves descend to about the same minimum values for slightly higher values of p before merging in close proximity with the curves shown. As a consequence, one will not err greatly in using the curves shown in Fig. 4.

Mean and Standard Deviation of $F_i(k, \tilde{\nu})$

The probability density of $\tilde{\chi}$ is simply the derivative of the distribution function (14a) or

$$f_{\tilde{\chi}}(z) = \frac{nz}{\sigma^2} p (1-p)^{n-1} \tag{15a}$$

where p is the complement Rayleigh distribution function. The various moments may be computed from the probability density function. Carrying out the indicated operations gives

$$\bar{\tilde{\chi}}/\bar{\chi} = n \sum_{j=0}^{n-1} \frac{(-1)^j}{(j+1)^{3/2}} \, _{n-1}C_j, \tag{15b}$$
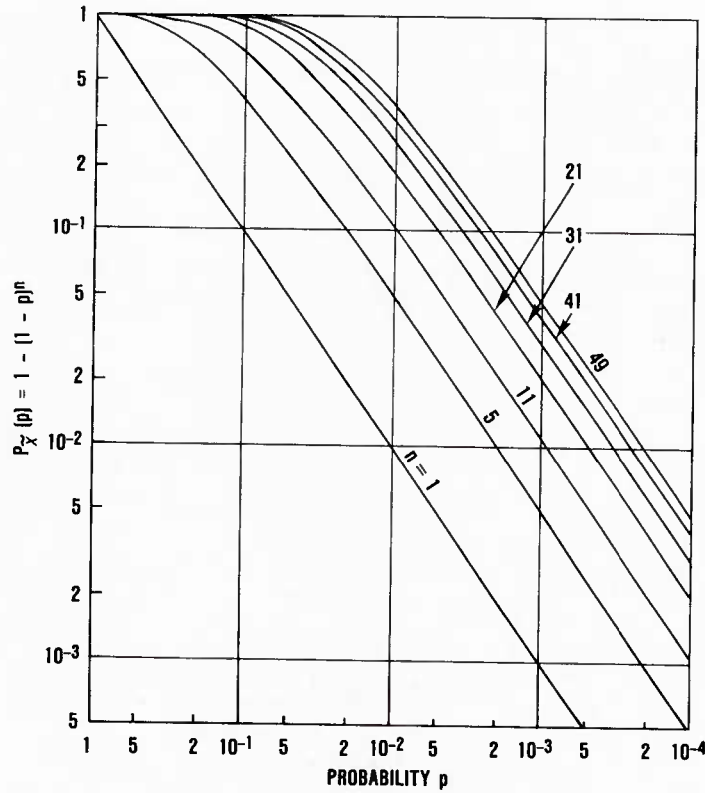
10

Fig. 4 — Complement distribution function of the CST peak output for a random Gaussian signal as a function of the complement Rayleigh distribution function, p. The curves assume the distribution functions of the CST at each ν are independent. At small values of p the curves approximate np, where n is the total number of cant values in the CST.
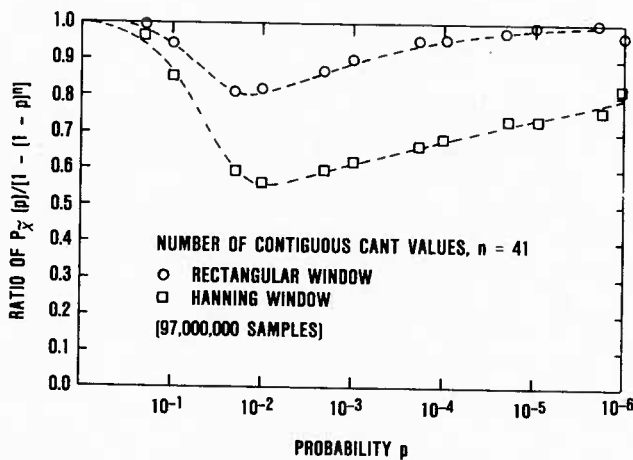

Fig. 5 — Experimentally determined deviations from the complement distribution function shown in Fig. 4 as a result of dependence between the cant values ν; $n=41$. The deviation for other values of n closely approximate those illustrated for p less than about 10^{-2}. As n gets smaller, however, the deviation tends to decay and reach approximately the same minimum for slightly larger values of p. It may be concluded that one will not err significantly by using the curves shown in Fig. 4 for the complement distribution function of the CST peak output.

and

$$\sigma_{\bar{\chi}}/\sigma_{\chi} = \left\{ \frac{1}{4-\pi} \left[4n \sum_{j=0}^{n-1} \frac{(-1)^j}{(j+1)^2} \,_{n-1}C_j - \pi \, (\bar{\bar{\chi}}/\bar{\chi})^2 \right] \right\}^{1/2}, \qquad (15c)$$

where $\bar{\chi}$ and σ_{χ} are the mean and standard deviation of the Rayleigh distributed CST statistic $\chi_j = F_i(k, \nu_j)$.

Figure 6 is a plot of the above functions along with experimental measures obtained from the CST by using a Gaussian noise signal. The experimental data reflect the dependence or covariance between the χ_j sample increments.
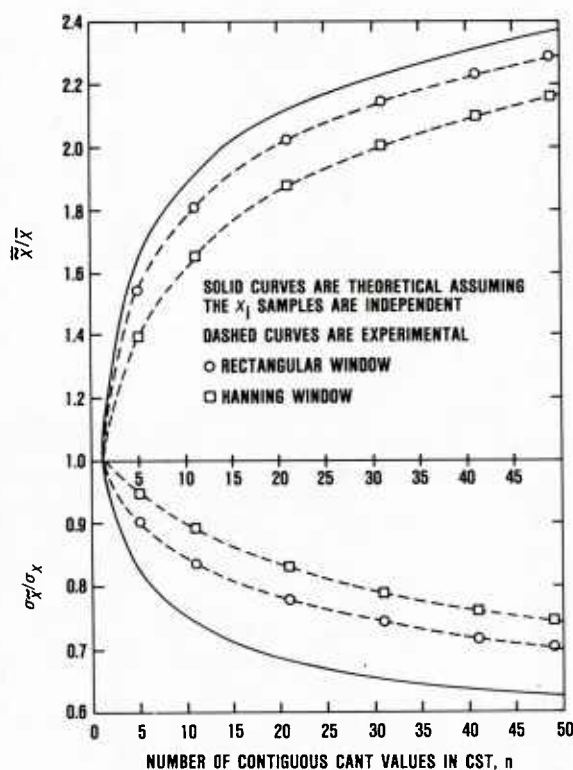
Fig. 6 — Mean and standard deviation of the peak CST output for a random Gaussian signal as a function of n, relative to the values for $n=1$. The theoretical curves assume independence between the cant values, while the dashed curves were obtained experimentally by averaging about 250,000 samples per point. Deviation from the theoretical curves is attributable to the dependence between cant values.

Characteristics of the Variable $\tilde{\nu}$

Experimental measures were made to determine the distribution of the statistic $\tilde{\nu}$ for a random Gaussian signal. This variable is the member of the set $\{\nu\}$ that maximizes the CST for a given input signal sample. The observed distribution of $\tilde{\nu}$ is uniform over the range of cants except at the two end points where the probability is higher than the mean. This implies that the covariance between the cant parameters are nonzero. In this event, maximum CST values, which would occur for ν values outside of the range of cants employed in the CST, will increase the probability that the maximum will occur at the nearest end point.

12

To verify the above hypothesis, the normalized covariance between χ_j and χ_{j+n}, from Eq. (13a), was computed experimentally. Figure 7 shows the results for both the rectangular and the Hanning windows. Clearly, a significant correlation exists between adjacent values of ν for the rectangular window, and for even greater separation of ν values in the case of the Hanning window. This further verifies that the use of other than the rectangular window is disadvantageous in the case of the CST. Computing the mean value and standard deviation of the CST, using a sequence of cant values separated 4 or greater apart, resulted in values that approached the theoretical curve shown in Fig. 6.
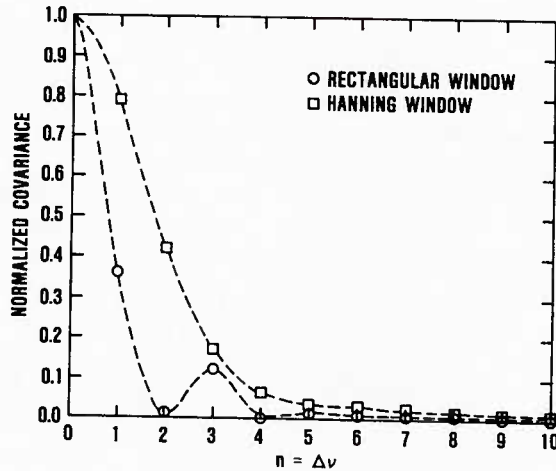

Fig. 7 — Normalized covariance between cant values as a function of the cant separation $\Delta\nu$ for rectangular and Hanning windows.

As a consequence of the covariance between neighboring values of the cant variable, the probability for the interior values of cant (exclusive of the end points) is somewhat less than the inverse of the total number of cants employed in the CST. From the standpoint of the probability distribution of the interior cant values, the effect of the cant dependence on its near neighbors is reflected as an effective increase in the number of cants employed. That is, if the total number of contiguous cants employed in the CST is n, the probability of the interior cants is such that they perceive $n + a$ independent values. And the probability of the interior points is $1/(n+a)$. To determine a suitable value for a, the distribution of ν was experimentally measured for n equal to 5, 11, 21, 31, 41, and 49 for both the rectangular and the Hanning window. It was determined that using values of a equal to 0.4 for the rectangular window and 1.4 for the Hanning window, the ratio $1/(n+a)$ very nearly equaled the experimentally determined values of probability for the interior cant points. The empirical relation is particularly good for n greater than about 10.

CST STATISTICS FOR A SIGNAL IN NOISE

Consider the canted spectral transform of a signal comprised of a linear frequency-modulated sinusoid and random Gaussian-distributed noise. Let

$$s_n = a \sin\left[\pi \frac{n}{N}\left(2k_0 + \nu_0 \frac{n}{N}\right)\right] + \eta_n, \tag{16}$$

where η_n is a zero-mean Gaussian variable with variance σ^2. Let $\chi_j = F_i(k, \nu_j)$ be a sample CST statistic for $\nu = \nu_j (j = 1, 2, \ldots, n)$, where k is chosen to include k_0 within its bin width of $+1/2$. Define $\tilde{\chi} = F_i(k, \tilde{\nu})$ such that $\chi_j \leqslant \tilde{\chi}$ for all j, and $\tilde{\nu}$ is a member of the set $\{\nu_j\}$. Of interest will be the distributions of $\tilde{\nu}$ as a function of the inband signal-to-noise ratio r and fractional offsets in the parameters k_0 and ν_0.

13

Experimental Parameters

The desired distributions were measured experimentally by using Eq. (16) in Eq. (3), for both a rectangular and a Hanning window. The CST parameters were; $N = 1024$, $k = 200$, and $\nu = -20$, $\cdots$, 0, $\cdots$, 20. The signal parameters included: $k_0 = 200$ and 200.5, $\nu_0 = -0.5$, 0, 9.5, and 10; and inband signal-to-noise ratio $r = 20$, 10, 6, 3, 0, -3, and -6 dB. Using Gaussian noise statistics, more than 20,000 samples of the CST statistic were obtained for each set of parameters in measuring the $\tilde{\nu}$ distributions. The $\tilde{\nu}$ distributions for Gaussian noise only were determined earlier.

Distributions of the Peak Cant $\tilde{\nu}$

As expected, the distributions of $\tilde{\nu}$ are independent of the parameter ν_0 as long as ν_0 is an interior cant within the range of the cants ν_j, and is not close to an end value. The distributions are dependent on the offsets of both k_0 and ν_0 from their nearest integer values. Figure 8 shows the distributions of $\tilde{\nu}$ as a function of the inband signal-to-noise ratio r, for a rectangular window and for fractional offsets of the parameters k_0 and ν_0. The upper left-hand diagram shows the distributions when both k_0 and ν_0 are integers. The upper right-hand diagram illustrates the effect of k_0 being offset by 1/2; that is to the edge of the k bin. The lower left-hand diagram illustrates the case where ν_0 is midway between two integer cants. And the lower right-hand diagram illustrates the case where both k_0 and ν_0 are offset by 1/2. From the figure, one can readily see that a cant shift of one nearly compensates for the degradation induced by the signal frequency occurring at the edge of the spectral bin. Further, the degradation resulting from the signal cant being midway between two integer cant values is partially compensated when the signal frequency is offset from the bin center. In practice, the values of k_0 and ν_0 can be expected to be uniformly distributed over $\pm 1/2$ from an integer value.

Figure 9 displays the distributions of $\tilde{\nu}$ as a function of the inband signal-to-noise ratio r, for a Hanning window and for fractional offsets of the two signal parameters. The rationale of the four diagrams is identical to that given for the case of the rectangular window. The distributions in the k bin do not differ greatly from those realized with the rectangular window. The peak values are approximately the same, although the distributions about the peak values are somewhat broader. This broadening effect about the peaks can be attributed to the broader bandwidth of the CST for a Hanning window. As evidenced from Figs. 1 and 2, the $\tilde{\nu}$ distributions for values of k remote from k_0 can be significantly different for the two window functions.

Cumulative Distributions of the Peak Cant $\tilde{\nu}$

The cumulative distribution of the peak cant is defined as the sum of the probabilities at 0 and about either side of zero on the abscissa scale in the diagrams in Figs. 8 and 9. That is, the cumulative distribution at a scale value of m is simply the probability at the scale value 0 plus the sum of the probabilities at both positive and negative scale values up to and including m. Using this definition, the cumulative distributions of the peak cant for the rectangular window are shown in Fig. 10. The rationale of the four diagrams is the same as that described for the earlier distributions. In the upper left-hand diagram, the cumulative distribution for r equal to 20 dB coincides with the vertical ordinate axis, and consequently is not perceived. It is, however, visible on the remaining three diagrams as illustrated in the upper right-hand diagram. As may be seen, the probability rises rapidly at a scale of one, after which it rises less rapidly with increased values of the abscissa scale. The cumulative distribution for a noise-only signal ($r = -\infty\,dB$) is simply a straight line as expected. These curves, as well as the earlier distributions represent the results for 41 contiguous values of the cant variable.

The cumulative distributions of the peak cant for the Hanning window are displayed in Fig. 11, with the same format as employed in Fig. 10. The curves for the Hanning window closely approximate those for the rectangular window. They generally rise more steeply at an abscissa value of one; after which they ascend more gradually. This behavior is attributed to the broader peaks of their distributions.
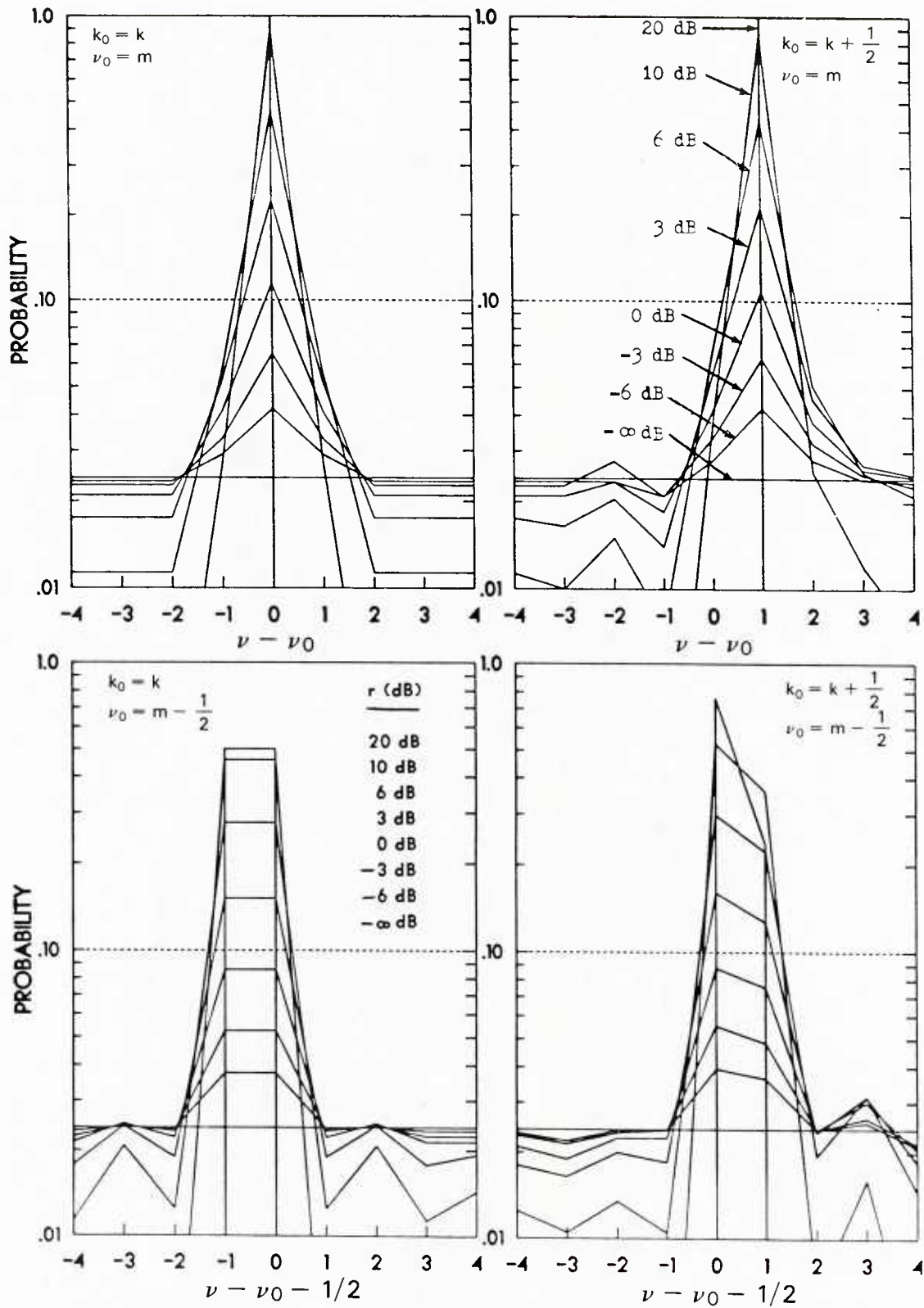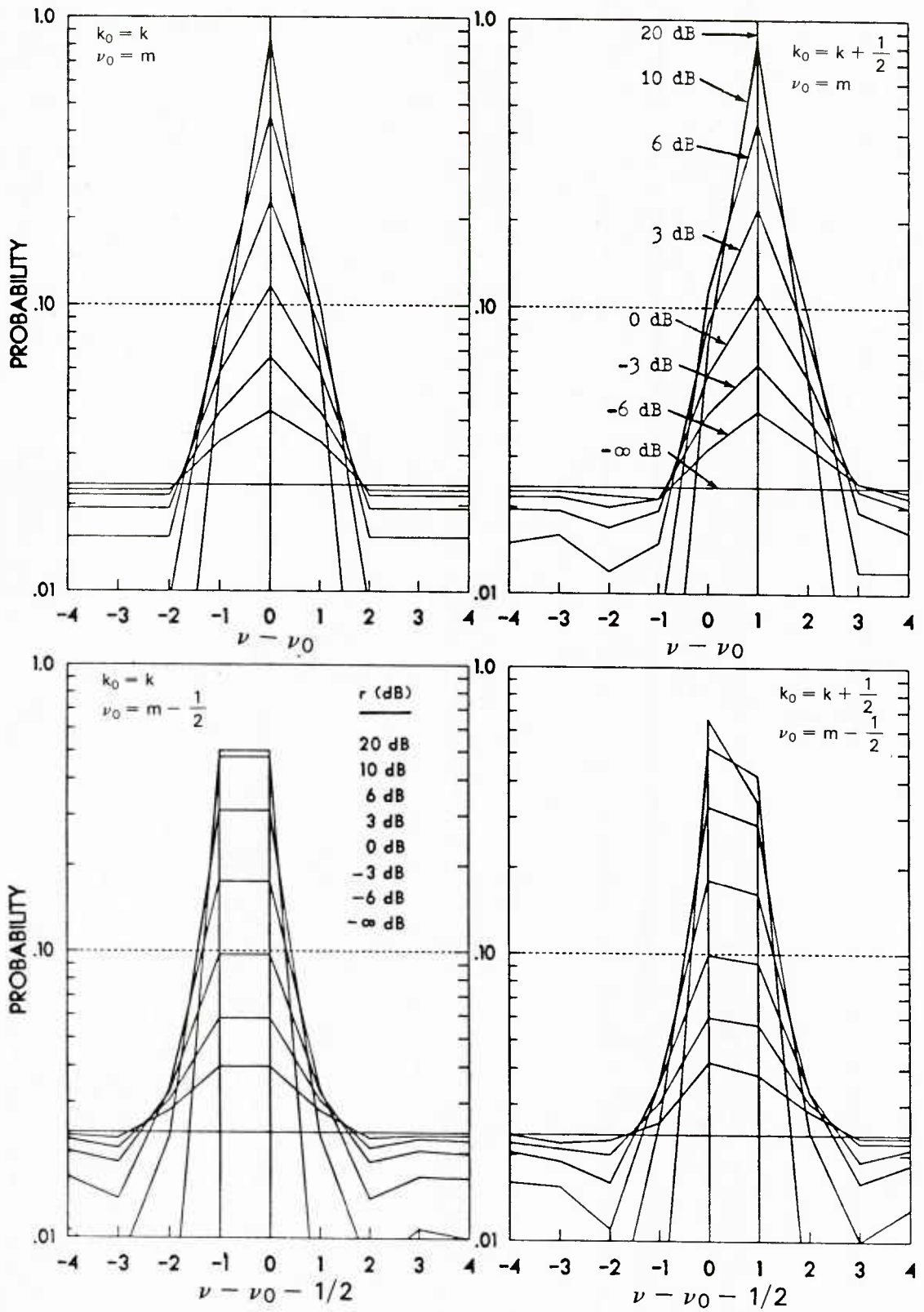
14

Fig. 8 — Distributions of the peak cant $\tilde{\nu}$ for a ramp-frequency signal in random noise, a rectangular window, and selected values of inband signal-to-noise ratio r. The upper left-hand diagram illustrates the case when the signal parameters k_0 and ν_0 are integers. In the upper right-hand diagram, ν_0 is an integer but k_0 is an odd multiple of $1/2$; that is, k_0 is at the bin edge. In the lower left-hand diagram, k_0 is in the center of the k bin but ν_0 is an odd multiple of $1/2$; that is, ν_0 is midway between two cant values. In the lower right-hand diagram, both k_0 and ν_0 are odd multiples of $1/2$. The number of contiguous cant values, in all cases, is 41.

Fig. 9 — Distributions of the peak cant $\tilde{\nu}$ for a ramp-frequency signal in random noise, a Hanning window, and selected values of inband signal-to-noise ratio r. The rationale for the four diagrams is the same as described in Fig. 8. The number of contiguous cant values, in all cases, is 41.
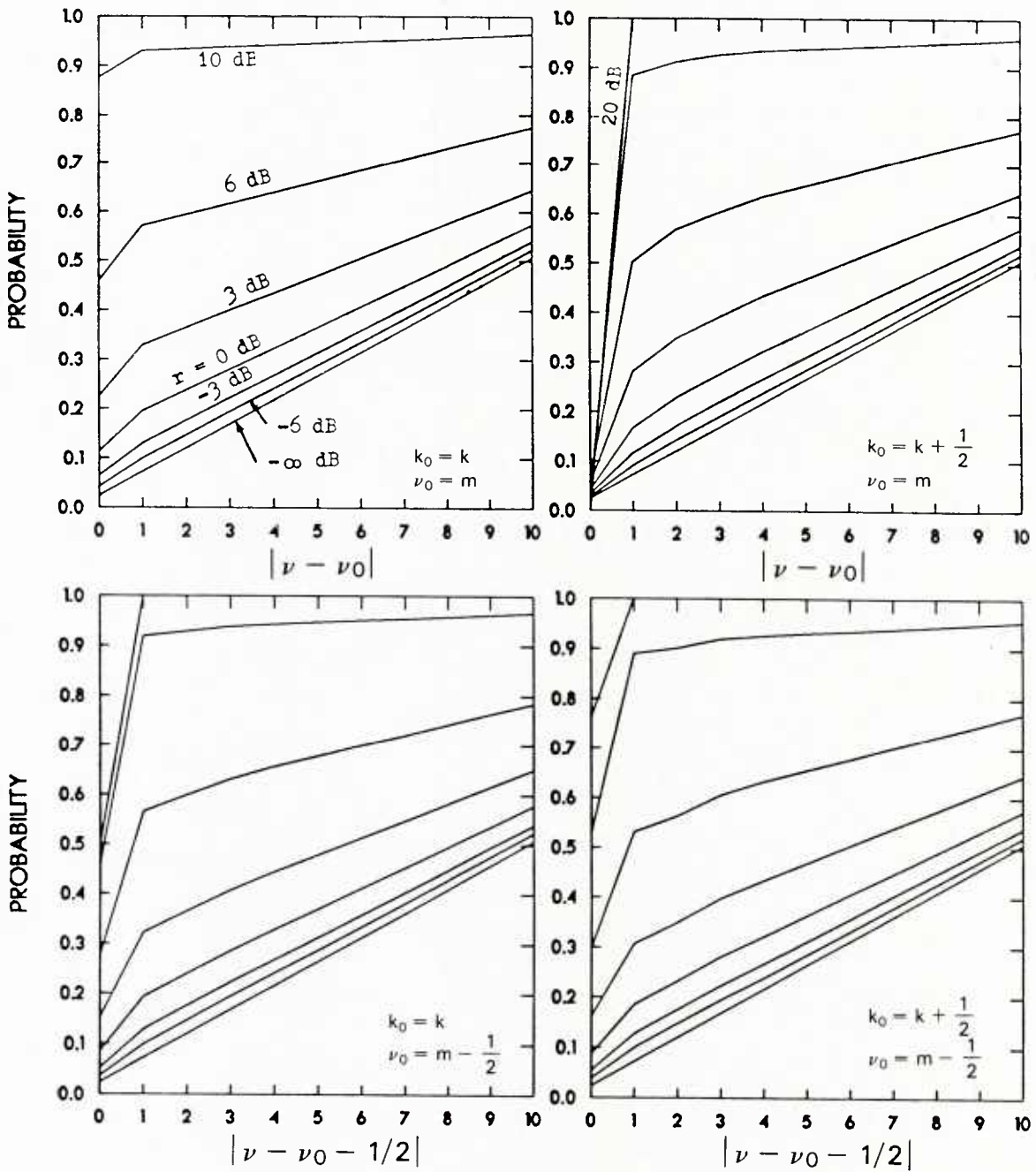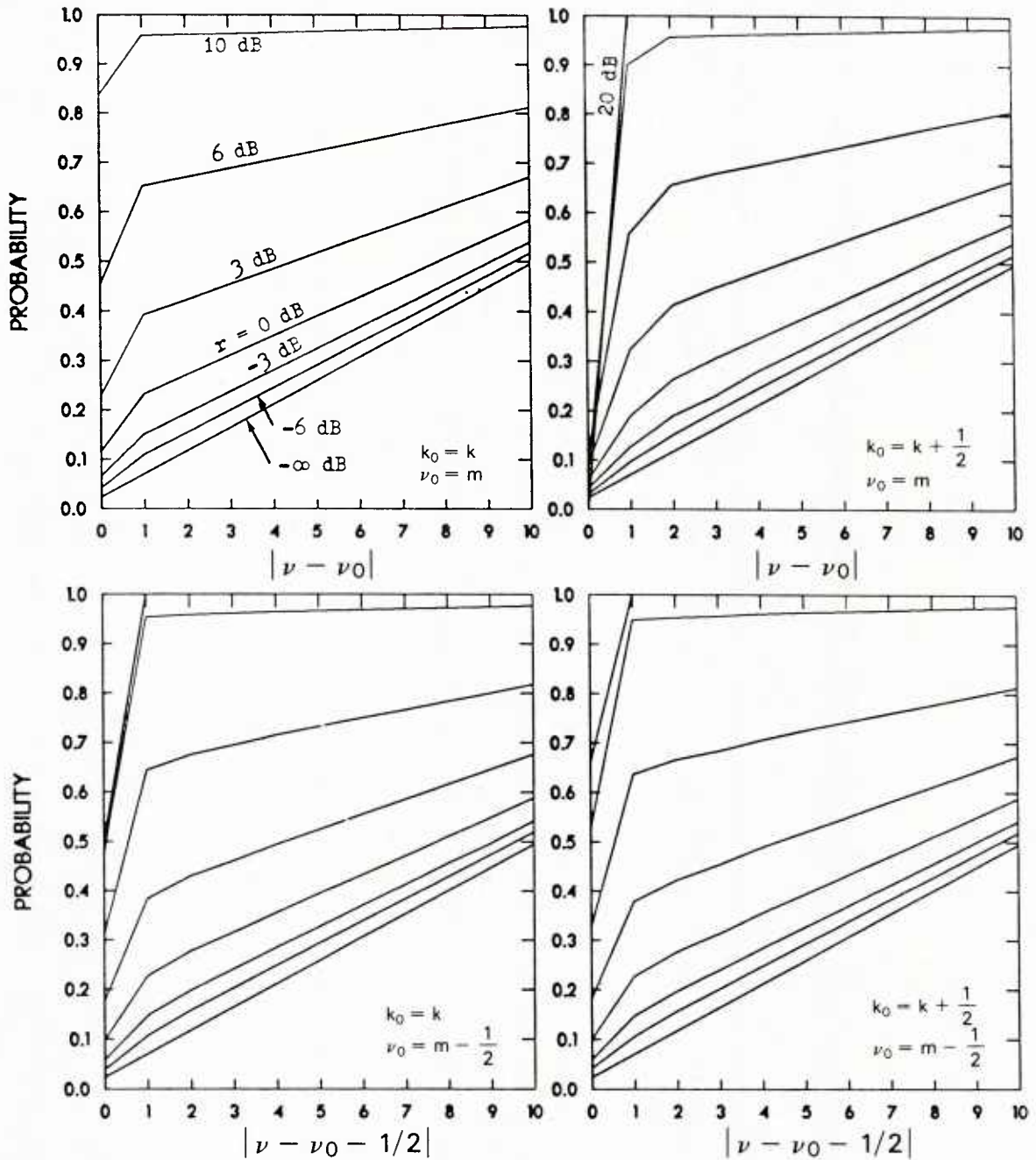
Fig. 10 — Cumulative distributions of the peak cant $\tilde{\nu}$ for a ramp-frequency signal in random noise, a rectangular window, and selected values of inband signal-to-noise ratio r. The rationale for the four diagrams is the same as described in Fig. 8. The number of contiguous cant values, in all cases, is 41. The cumulative distributions are computed from the data in Fig. 8 by summing the probabilities for the abscissa scale value of 0 and the absolute scale values about 0 up to the indicated scale value.

Fig. 11 — Cumulative distributions of the peak cant $\bar{\nu}$ for a ramp-frequency signal in random noise, a Hanning window, and selected values of inband signal-to-noise ratio r. The rationale for the four diagrams is the same as described in Fig. 8. The number of contiguous cant values, in all cases, is 41. The cumulative distributions are computed from the data in Fig. 9 by summing the probabilities for the abscissa scale value of 0 and the absolute scale values about 0 up to the indicated scale value.

It is well to remember that all of the distributions shown in Figs. 8 through 11 are truly discrete values and not continuous. Straight lines between the discrete values of probability have been drawn for convenience in displaying the results.

SUMMARY AND CONCLUSIONS

The conventional sectionalized Fourier transform (SFT) accumulates signal energy in narrow spectral channels or frequency bins that are constant over the integration time of the transform. It has been shown that by extending the phase kernel of the SFT, signal energy over narrow spectral channels that vary dynamically over the integration period can be accumulated to achieve optimum detection sensitivity for a narrowband signal whose instantaneous-frequency dynamics are known. When the spectral dynamics of the signal are unknown, the parameters of the generalized kernel may be varied to obtain estimates of the input signal-frequency dynamics. The canted spectral transform (CST), which employs a quadratic phase kernel (or Fourier-Fresnel kernel), is an initial step toward achieving a generalized spectral transform.

The statistical properties of the CST reveal that shaded window functions are generally inferior to the rectangular window (commonly referred to as no window) in discriminating the cant of signals whose instantaneous frequency varies linearly with time. Although the primary utility of the CST is in detecting signals with linearly varying frequency characteristics, it also has merit as a conventional spectrum analyzer by appropriately exploiting the distribution characteristics of the peak cant variable. The statistical properties of the CST for both signal and noise provide a basis for determining the performance of the transform in practical applications.

ACKNOWLEDGMENTS

REFERENCES

1. J.W. Cooley and J.W. Tukey, "An Algorithm for the Machine Calculation of Complex Fourier Series," *Math. Comput.* **19**, 297-301 (1965).

2. W.T. Cochran, J.W. Cooley et al., "What is the Fast Fourier Transform?," *IEEE Trans. Audio Electroacoust.* **AU-15**, 45-55 (1967).

3. G.C. Carter, C.H. Knapp, and A.H. Nuttall, "Estimation of the Magnitude-Squared Coherence Function via Overlapped Fast Fourier Transform Processing," *IEEE Trans. Audio Electroacoust.* **AU-21**, 337-344 (1973).

4. R.D. Trueblood and D.L. Alspach, "Multiple Coherence as a Test Statistic," NOSC Rpt. TR-265, July 1978.

5. A.A. Gerlach, "Role of the Sectionalized Fourier Transform in High-Speed Coherence Processing," NRL Report 8438, Oct. 1980.

6. A.A. Gerlach, "High-Speed Coherence Processing Using The Sectionalized Fourier Transform," *IEEE Trans. Acoust. Speech Processing* **ASSP-26**(2), 189-205 (1982).

7. J.J. Wolcin, "Maximum a Posteiori Estimation of Narrow-band Signal Parameters," *J. Acoust. Soc. Am.* **68**(1), 174-178 (1980).

8. George Rogers, TRW, Inc., Private communications (1984).

9. R.V. Hogg and A.T. Craig, *Introduction to Mathematical Statistics*, 2nd ed. (The Macmillan Company, New York, 1965) Ch. 6, pp. 168-175.

U227807